Earthquake Geotechnical Engineering for Protection and Development of Environment and Constructions – Silvestri & Moraci (Eds)
© 2019 Associazione Geotecnica Italiana, Rome, Italy, ISBN 978-0-367-14328-2

Next generation reduced order models for soil-structure interaction

D. Asimaki, J. Garcia-Suarez, D. Kusanovic, K. Nguyen & E. Esmaeilzadeh Seylabi
Mechanical & Civil Engineering, California Institute of Technology, Pasadena, U.S.A.

ABSTRACT: A number of published solutions have been dedicated to problems of dynamic soil-structure interaction (SSI) for geotechnical infrastructure over the past 50 years. Some have been formulated using idealized models with a number of severe assumptions based on physical intuition. Others have been developed by fitting large-scale experimental results or back-calculated from field measurements. Their simplified formulation and wide use notwithstanding, reliable predictions of such models are guaranteed so long as the geometry, material properties and loading conditions of the problems at hand match the reference configurations. Over the past decade, we have worked on developing SSI reduced order models (ROMs) based on rigorous mechanics, intended to expand the range of their applicability to conditions outside the range of numerical and physical experiments used to formulate them. In this paper, we present three examples: a framework based on small parameters, energy and momentum balance to resolve soil-structure on rigid retaining walls; a two-dimensional linear ROM for transient analysis of (nonlinear) buildings on mat foundations in a homogeneous half-space; and a two-dimensional nonlinear ROM for the transient analysis of pipeline systems subjected to transient ground deformation. We will specifically highlight the physics of each problem as revealed by formalized mechanics solutions and high-fidelity simulations; present reduced order models that capture salient aspects of the physics; and show comparisons of our model predictions to state-of-the art methodologies.

1 INTRODUCTION

In complex urban environments, earthquake resilient design of transportation infrastructure, pipeline networks and building structures is not an isolated target; rather, it involves minimizing damage, loss, and recovery time of the system themselves, but also limiting the number of cascading disasters that can stem from or affect the said systems. Thus, design procedures that evaluate the risk associated with a range of hazard scenarios call for a large number of simulations, considering –among other complex phenomena– soil-structure interaction (SSI) effects. Today, one can perform high-fidelity simulations for analysis of complex SSI problems (e.g., Vazouras et al., 2010) and can use data from small to large scale experiments and infrastructure instrumentation to achieve a better understanding of the system behavior, intended to inform high-fidelity numerical models (e.g., Lanzano et al., 2012). Nonetheless, the computational cost of high fidelity SSI simulations continues to loom large, particularly for nonlinear fully coupled models, an obstacle which, combined with the large number of analyses needed to make fully probabilistic risk predictions, can render the problem intractable. Lower (or equivalent) fidelity predictive models, namely models that can capture the main features of high-fidelity simulations at reduced computational cost, are therefore essential, especially in probabilistic engineering and resilient design of interconnected civil infrastructure systems.

Developing lower fidelity predictive models for SSI problems usually relies on replacing the surrounding soil by reduced order models (ROMs) while keeping the structure intact. The soil ROM is a nonlinear spatio-temporal map that translates the transient ground deformations (TGD) to the traction resultants along the soil-structure interface. Although a large number of ROMs have been previously proposed to quantify SSI effects, most have been formulated

in the frequency-domain, and are restricted either by oversimplifying assumptions (e.g., Veletsos and Meek, 1974; Jacobo, 1975) or by relying on superposition (e.g., Stewart et al., 1999, 2012; Givens et al., 2016) to a limited class of linear elastic problems.

Over the past decade, we have worked on developing ROMs based on rigorous mechanics, intended to expand the range of their applicability. In this paper, we provide a taste of the methodologies we use to develop ROMs for different SSI problems, i.e., for retaining walls, building structures and pipelines. For each case, we present the physics of the problem, the existing drawbacks of the state-of-research, and the methodology we use for reduced order modeling. We also briefly discuss the performance of the derived models in reproducing the quantities of interest in high fidelity models.

2 RETAINING WALLS

The interest in understanding how soils exert pressure on retaining walls dates back more than two-hundred years. Coulomb developed his static method, based on what is called today the Limit-State Theory, back in the 18th century. A natural extension of his approach intended to be used in the setting of dynamic loading induced by seismic events was presented in the 1920s by Mononobe and Okabe (popularly referred as ``M-O method''). This method remains popular nowadays in spite of presenting a number of drawbacks: (1) being a quasi-static equivalent method, with all the caveats that neglecting dynamics that it carries along; (2) an issue inherited from Limit-State theory, namely that the method presupposes a certain level of displacement of the wall necessary to induce plastic behavior in the backfill; (3) as it is a method based on free-body equilibrium instead that on deformation considerations, it can estimate total thrust acting on the wall yet not the pressure distribution along the wall. Due to these, neither frequency-dependent behavior (resonance) can be captured in the model nor pressure distribution on not-sliding walls is suitable to be characterized.

To make up for these shortcomings, throughout the years, many relevant contributions have been presented. Scott (1973) proposed the concept of soil springs *between far-field and the wall* as a way of relating soil behavior in the far-field, e.g. *very far from the wall* (as far as to not to be influence by the presence of wall) to the soil behavior *on the wall*. He recognized that soil movement, or lack thereof, entails the onset of stresses in the soil, which in turn translates into distribution of pressures acting on the wall in contact to the soil. Through this simple idea, the effect of the intermediate soil region is idealized as a series of springs whose relative stretching between the wall and the far-field induces the stress state at the wall. This idea of spring-like behavior of the intermediate soil mass was picked up by the next generation of researchers, who quickly extended it to the dynamic setting turning it into an impedance (dynamic stiffness), that accounts for frequency-sensitivity and for soil damping (e.g., Veletsos and Younan, 1994; Kloukinas et al., 2012; Brandenberg et al., 2015).

However, all the aforementioned contributions rely on over-simplifying assumptions on stresses and boundary conditions to derive a final result. In order to improve the state-of-research for computing the impedance functions for retaining walls, we worked on relaxing the strong assumptions that are commonly used, and resorted to non-conventional analytic tools–i.e., dimensional analysis, energy balance by means of the J-integral, and asymptotic analysis in presence of small parameters. These analytic tools are customary to other fields of Continuum Mechanics but have not previously been utilized in the study of this problem.

Figure 1 shows the schematic of the problem under consideration. Under the optics of Dimensional Analysis, we can show that, in the quasi-static/long-wavelength excitation regime, there are only two length scales involved in the problem: the height of the wall H and $\ell_s = \mu/\rho\gamma = V_s^2/\gamma$ where $H << \ell_s$, V_s is the soil shear wave velocity, ρ is the soil mass density, and γ is the amplitude of the earthquake excitation. Whatever the solution is, it must depend on this two parameters. It is also acknowledged that $H/\ell_s << 1$, for natural values of the parameters. considerations in terms of Energy Balance are pursued. These were absent from previous research efforts, as it was unclear that possible approaches could deliver any useful result that could inform ways of simplifying the problem. Moreover, inspired by Fracture

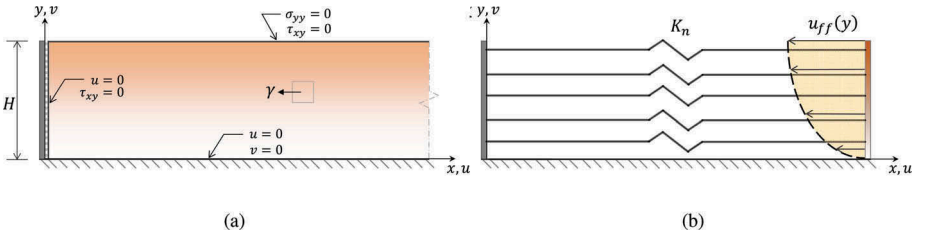

Figure 1. (a) scheme of the 2D plane-strain retaining wall problem under consideration. (b) modelization of the reduced order model.

Mechanics (Rice, 1968), we exploit the divergence-free nature of the Eshelby energy-momentum tensor $\bar{E}_{ij,j}$ (properly adapted to account for the presence of a body force in the problem) to define a null contour-independent integral over the domain. That is,

$$\bar{E}_{ij} = (W + u_k b_k)\delta_{ij} - u_{k,i}\sigma_{kj} \rightarrow \bar{E}_{ij,j} = 0 \rightarrow J_i = \int_D \bar{E}_{ij,j} dS = \int_\Gamma (\bar{E}_{ix} dy - \bar{E}_{iy} dx) = 0 \qquad (1)$$

where b_k represents the entries of the vector of body forces ($b_x = \rho\gamma$ and $b_y = 0$ but also $b_{k,j} = 0\ \forall k$), W represents the strain energy density and Γ is any closed contour defined over the soil domain D (the equivalence between the surface integral and the contour integral is just a consequence of Green's theorem). The divergence-free nature of $\bar{E}_{ij}$ is a consequence of the quasi-static equilibrium equations rice1968path. These identities set a relation between the components of the displacement field (and its gradients) in each part of the contour (base of the stratum, far-field, layer surface and wall). Our physical interpretation of this integral is: as the earthquake is introducing a certain amount of energy in the system (portrayed in this model as the work of the fictitious body force), such energy must translate into a stress/strain state, but it does it differently in different regions of the model as the boundary conditions are different as well. Regardless of how different the conversion is in each region, they must be related so that the final sum is balanced. The most interesting observation about these identities is that they precede any simplification assumed over the system, therefore, a good way of testing the fitness of any reduced model is checking if it abides by the identities in spite of simplifications. If that was not the case, it seems appropriate to believe that the simplified models do not capture the fundamental physics of the problem. Finally, we use asymptotic analysis to guide us simplifying the equations of motion in different regions of the problem. The equations of motion are (harmonic loading is assumed)

$$(\lambda + 2\mu)\frac{\partial^2 u}{\partial x^2} + (\lambda + \mu)\frac{\partial^2 v}{\partial x \partial y} + \mu\frac{\partial^2 u}{\partial y^2} = \rho\frac{\partial^2 u}{\partial t^2} + \rho\gamma e^{i\varpi t} \qquad (2a)$$

$$(\lambda + 2\mu)\frac{\partial^2 v}{\partial y^2} + (\lambda + \mu)\frac{\partial^2 u}{\partial x \partial y} + \mu\frac{\partial^2 v}{\partial x^2} = \rho\frac{\partial^2 v}{\partial t^2} \qquad (2b)$$

For this problem setting, the introduced dimensionless parameters are

$$\eta = \frac{y}{H} \quad \tilde{x} = \frac{x}{\ell_s} \quad \xi = \frac{x}{H} \quad \tilde{u} = \frac{u}{H\frac{H}{\ell_s}} \quad \tilde{v} = \frac{v}{H\frac{H}{\ell_s}} \quad c = \sqrt{\frac{\lambda + 2\mu}{\mu}} \quad r = \frac{\varpi}{c_s/H} \qquad (3)$$

where μ and λ are Lame's constants. We begin by recognizing that there is no clear length scale when it comes to consider the horizontal direction, unlike in the vertical direction, where

changes happen clearly along spans $\Delta y \sim H$. Thus, we may argue that, at least in the region that is not directly affected by the wall, no meaningful changes are appreciated as relatively short spans are traversed in horizontal direction. A way of translating this fact to mathematical terms is assuming that $\Delta x \sim \ell_s$, as ℓ_s is the largest length-scale present in the problem. Rewriting the equations in non-dimensional form, the small parameter $\varepsilon = H/\ell_s$ springs out in front of terms involving derivatives with respect to x, which indicates that the solution of the problem is equal to the solution at the far-field up to terms $\mathcal{O}(\in)$.

$$c^2\varepsilon^2\frac{\partial^2\tilde{u}}{\partial\tilde{x}^2} + (c^2-1)\varepsilon\frac{\partial^2\tilde{v}}{\partial\tilde{x}\partial\eta} + \frac{\partial^2\tilde{u}}{\partial\eta^2} = r^2\frac{\partial^2\tilde{u}}{\partial\tau^2} + e^{i\tau} \tag{4a}$$

$$c^2\frac{\partial^2\tilde{v}}{\partial\eta^2} + (c^2-1)\varepsilon\frac{\partial^2\tilde{u}}{\partial\tilde{x}\partial\eta} + \varepsilon^2\frac{\partial^2\tilde{v}}{\partial\tilde{x}^2} = r^2\frac{\partial^2\tilde{v}}{\partial\tau^2} \tag{4b}$$

Next, it is acknowledged that the mathematical structure of the equation is that of a Boundary Layer connected to the wall. By stretching the x-coordinate, H is found to be the layer width. This fact indicates that the influence of the wall on the solution must be limited to a distance $\sim H$ from the wall, while the rest of the domain effectively behaves as the far-field. The equilibrium equations in this region are

$$c^2\frac{\partial^2\tilde{u}}{\partial\xi^2} + (c^2-1)\frac{\partial^2\tilde{v}}{\partial\xi\partial\eta} + \frac{\partial^2\tilde{u}}{\partial\eta^2} = r^2\frac{\partial^2\tilde{u}}{\partial\tau^2} + e^{i\tau} \tag{5a}$$

$$c^2\frac{\partial^2\tilde{v}}{\partial\eta^2} + (c^2-1)\frac{\partial^2\tilde{u}}{\partial\xi\partial\eta} + \frac{\partial^2\tilde{v}}{\partial\xi^2} = r^2\frac{\partial^2\tilde{v}}{\partial\tau^2} \tag{5b}$$

Last equations indicate that all the entries of the stress tensor in this region are, a priori, of the same order of magnitude, which precludes simplifications based on ignoring some stress components.

At the interface between the wall and the soil, the solution is directly controlled by the boundary conditions on the wall. Using the above mentioned tools, we found that for the specific case of a smooth and rigid wall, the *first-order* equilibrium in horizontal direction and the equilibrium in vertical direction *on the wall*, in the quasi-static/long-wavelength setting, is

$$c^2\frac{\partial^2\tilde{u}}{\partial\xi^2} = r^2\frac{\partial^2\tilde{u}}{\partial\tau^2} + e^{i\tau} \tag{6a}$$

$$c^2\frac{\partial^2\tilde{v}}{\partial\eta^2} + (c^2-1)\frac{\partial^2\tilde{u}}{\partial\xi\partial\eta} + \frac{\partial^2\tilde{v}}{\partial\xi^2} = r^2\frac{\partial^2\tilde{v}}{\partial\tau^2} \tag{6b}$$

As a conclusion, when $x/H \to 0$, the equilibrium in x-direction depends only on changes in the horizontal displacement, and the same thing happens when $x/H \to \infty$, although is not the case when $x/H \sim 1$. This leads to a simplification of the horizontal equilibrium equation at the soil-wall interface, that passes to depend only on horizontal displacement. However, if the equation is not tuned, the model would not abide by the restrictions imposed by the J-integral. To do that, we introduce a compressibility factor κ, which will be in charge of guaranteeing that the identity $J_1 = 0$ is verified. The new equations and the anticipated expression for κ, for the quasi-static/long-wavelength setting, are found to be

$$\frac{1}{\kappa^2}\frac{\partial^2\tilde{u}}{\partial\xi^2} + \frac{\partial^2\tilde{u}}{\partial\eta^2} = 1 \tag{7a}$$

$$c^2\frac{\partial^2\tilde{v}_w}{\partial\eta^2}+\frac{\partial^2\tilde{v}_w}{\partial\xi^2}=-(c^2-1)\frac{\partial}{\partial\eta}\left(\frac{\partial\tilde{u}}{\partial\xi}|_w\right) \tag{7b}$$

$$\text{s.t.}\quad \kappa(\nu)=\sqrt{\frac{1-\nu}{(\frac{192G^2}{\pi^4}-1)\nu+96\frac{G^2}{\pi^4}(\frac{7A}{2\pi G}-1)+\frac{3}{2}}} \tag{7c}$$

where we introduce a compressibility factor κ, which is in charge of guaranteeing that the identity $J_x=0$ is verified (in other words, it is guaranteed that this simplified model will abide by the restrictions imposed by energy balance); G represents the Catalan's constant catalan, A the Apery's constant (Weisstein, a), and ν the Poisson's ratio. This equation can be solved resorting to the vibration shapes at the far-field and once the horizontal displacement is known, the vertical displacement at the wall (soil sliding over the wall) can be found. Once the displacement field at the wall has been characterized, computing strains, stresses and thrust is straightforward. Although not shown for brevity, the static solution of Equation (7) agrees to the traditional exact solution derived by Wood (1973) for an equivalent problem (substantially more involved), and the dynamic solution reveals that the thrust is sensitive to a set of natural frequencies other than the natural frequencies of the infinite stratum. These new findings revealed by the new solution are confirmed by numerical simulations. We can use this new solution to compute the soil impedance functions along the height of the retaining wall. To do so, we observe that

$$\frac{u_{ff}(\eta)}{H\frac{H}{\ell_s}}=-\sum_{n=1}^{\infty}\frac{2}{k_n^3}\sin(k_n\eta) \tag{8}$$

$$\frac{\sigma_{xx}|_w(\eta)}{\rho\gamma H}=-\kappa(\nu)\sum_{n=1}^{\infty}\frac{2}{k_n^2}\left[\left(\frac{2-\nu}{1-\nu}\right)\sin(k_n\eta)+\left(\frac{\nu}{1-\nu}\right)(-1)^{n+1}\right] \tag{9}$$

where $k_n=(2n-1)\pi/2$ for $n=1,2,3,\ldots$; The displacement in the far-field comes expressed in terms of the vibration shapes $\sin(k_n\eta)$, yet the stress distribution on the wall does not. This precludes the existence of a material constant, independent of depth, relating the two of them. This fact seems to rule out the possibility of a definition of impedance, in the traditional sense, based on our solution. using the relation between series $\sum_{n=1}^{\infty}\frac{2}{k_n^2}(-1)^{n+1}=\frac{8G}{\pi^2}\sim\frac{8G}{\pi^2}\sum_{n=1}^{\infty}\frac{2}{k_n}\sin(k_n\eta)$ allows us to define the modal impedance function K_n relating each mode of free-field displacement u_{ff} to the earth pressure on the retaining wall.

$$\frac{\sigma_{xx}|_w}{\rho\gamma H}\sim\sum_{n=1}^{\infty}-\frac{2}{k_n^3}\sin(k_n\eta)\underbrace{\left[\kappa(\nu)k_n(\left(\frac{2-\nu}{1-\nu}\right)+\left(\frac{\nu}{1-\nu}\right)\frac{8G}{\pi^2}k_n^2)\right]}_{\frac{K_n}{\mu/H}} \tag{10}$$

$$\rightarrow K_n=k_n\left[\left(\frac{2-\nu}{1-\nu}\right)+\left(\frac{\nu}{1-\nu}\right)\frac{8G}{\pi^2}k_n\right]\kappa(\nu)\frac{\mu}{H}. \tag{11}$$

This expression for the impedance would yield an exact thrust in spite of not yielding the stress distribution everywhere. Figure 2 compares these new modal impedance functions against those previously proposed by Scott (1973); Veletsos and Younan (1994); Kloukinas et al. (2012). Note that K_n does depend on κ and this parameter depends on the boundary conditions on the wall.

Note that K_n does depend on κ and this parameter depends on the boundary conditions on the wall.

3 BUILDING STRUCTURES

ROMs for quantifying SSI effects in building structures are usually developed based on (semi-)analytical impedance functions (or dynamic springs) available for rigid foundations with simplified configurations (e.g., Pais and Kausel, 1988; Gazetas., 1991). Among other drawbacks associated with the existing models, their distribution along the building foundation is cumbersome, and by extension, so is their use for buildings with large, complex footprints that do not conform to the original simplified configurations. Moreover, integrating the impedance values in time-domain analyses of soil-foundation-structure interaction by selecting a representative, frequency-independent value, is not clear.

In this approach, we do not wish to challenge how impedance functions and their distribution along the foundation are employed to model dynamic SSI. Rather, our intention is to provide a numerical framework that enables users to compute the expression of impedances that account for the building, the foundation, and the surrounding soil simultaneously, and can be extended to the nonlinear regime and time-domain structural analysis solutions. We account for all the above phenomena using a series of uniformly distributed springs and dashpots, which reflect the aggregate stiffness and energy dissipation characteristics of the soil system as seen from the building foundation; and we *learn* the model coefficients of the springs and dashpots using data (real or synthetic) that incorporate all above mechanisms of interaction. In this particular application of the framework, we use high-fidelity models to learn the coefficients of the these elements. For high fidelity simulations (cf. Figure 3a), we consider a building structure with first modal height of h and fundamental period of T in the fixed-base condition which is supported by a foundation system of half-width B, and depth D, resting on a soil characterized by its shear-wave velocity V_s. We do not consider any viscous damping in the building nor the soil so that the energy loss as seen by the building is solely because of radiation damping.

To optimize the number of high-fidelity models to capture the physics of the problem, we employ Dimensional Analysis using the Buckingham Π-theorem (Buckingham, 1914). Accordingly, we obtain ten dimensionless parameters from which we consider only three to span dimensional parameter space. These three parameters are structure-to-soil stiffness ratio: $\Pi_1 = h/V_s T$, building-aspect ratio: $\Pi_2 = h/B$ and foundation-aspect ratio: $\Pi_3 = D/B$. In this regard, we use such parameters to define three different buildings with fixed base fundamental period $T \sim (0.5, 1.0, 1.5)$ s, fixed first modal height $h \sim (15.0, 30.0, 40.0)$ m, foundation depth $D = (1.0, 2.5, 5.0)$ m, and supported on eleven soil profiles with shear wave velocities $V_s = (80, 100, 125, 150, 175, 200, 225, 250, 300, 400, 500)$ m/s to capture several different

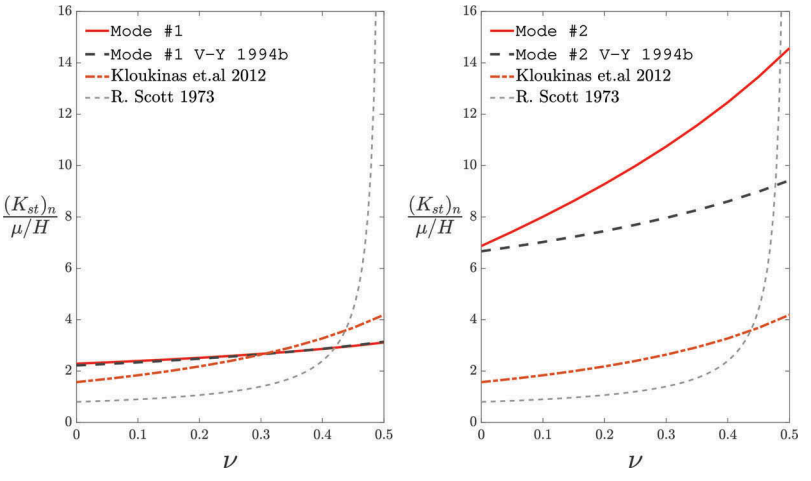

Figure 2. Comparison of newly derived impedance to prior results.

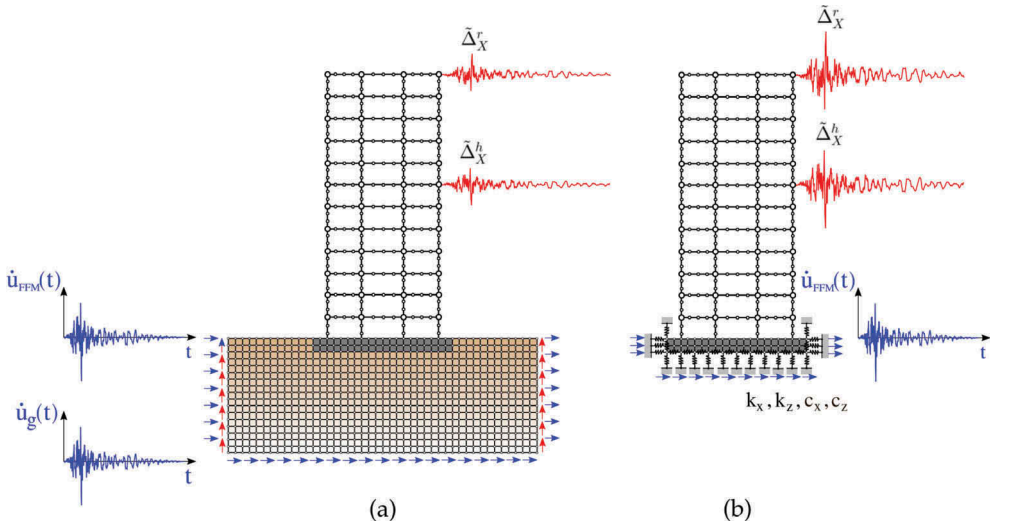

Figure 3. System-identification framework applied to SSI problem (a) Direct method from which the true responses are computed, and (b) Substructure method from which the spring and dashpot coefficients are estimated.

responses on the building due to different soil-foundation-building configurations. In this reduced parameter space, $\Pi_1 \in [0.05 - 0.4]$, $\Pi_2 \in [1.5 - 4.0]$ and $\Pi_3 \in [0.0 - 0.5]$, which covers the range of applicability in civil engineering.

For each configuration, we obtain the response of the high-fidelity model under vertically incident SV waves as shown in Figure 3a using the methodology suggested by Lysmer and Asimaki. Then, we use the resulting displacement and acceleration time-series at each floor along with a sequential optimization method based on extended Kalman filtering (Simon, 2006; Law et al., 2016) to update the coefficients of the springs and dashpots (cf. Figure 3b) such that the response error between the high-fidelity and reduced order models is minimized.

The responses of the building in the high-fidelity simulations guarantee that information of higher modes as well as SSI effects (for instance, period elongation and radiation damping) are present in the so-generated data; therefore, this approach ensures that such information is explicitly considered in the estimation of the coefficients of the uniformly distributed springs and dashpots. While the soil spring and dashpot coefficients identified in this manner are frequency independent, we consider this constraint acceptable since the earthquake time-series carry most of the energy in the range 0.2 10 [Hz], where the impedances of a half-space can be considered constant. On the other hand, this approach allows us to obtain the frequency at which the soil springs and dashpots in the ROM best describe the frequency of vibration of the high-fidelity model.

After estimation of the coefficients for each case in the dimensional parameter space, i.e., 99 cases, we employed a non-linear optimization on the ensemble of identified parameters to find a relation between the dimensionless parameters of the problem and the coefficients of the ROM. The non-linear function that interpolates the parameters of the distributed dynamic springs is given as:

$$S_i(\hat{\pi}, \hat{\alpha}, \hat{\beta}) = \lambda_i \, G(\hat{\beta}, B) \, F_i(\hat{\pi}, \hat{\alpha}) \,, \tag{12}$$

where the function $S_i(\hat{\pi}, \hat{\alpha}, \hat{\beta})$ on the left-hand side represents the i-th coefficient to be estimated; the non-linear function $F_i(\hat{\pi}, \hat{\alpha})$ represents the i-th SSI effect for a given configuration; the function $G(\hat{\beta}, B)$ represents the *foundation influence coefficient*. $\hat{\pi}$ is the *vector of*

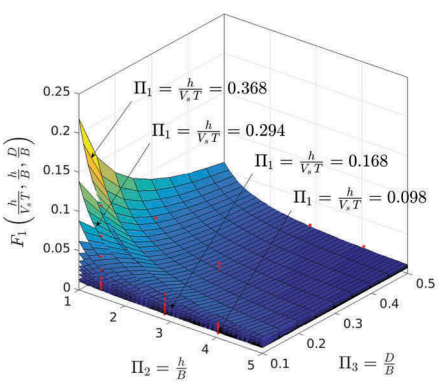

(a) Normalized soil-structure-interaction function $F_1(\hat{\boldsymbol{\pi}}, \hat{\boldsymbol{\alpha}})$ for the horizontal spring coefficient k_x.

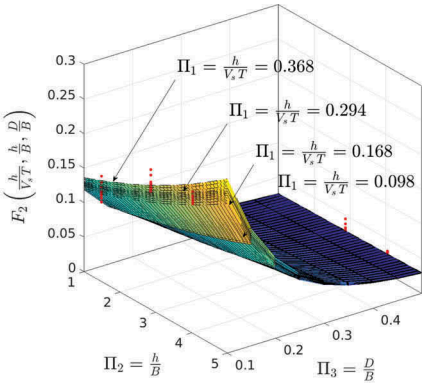

(b) Normalized soil-structure-interaction function $F_2(\hat{\boldsymbol{\pi}}, \hat{\boldsymbol{\alpha}})$ for the vertical spring coefficient k_z.

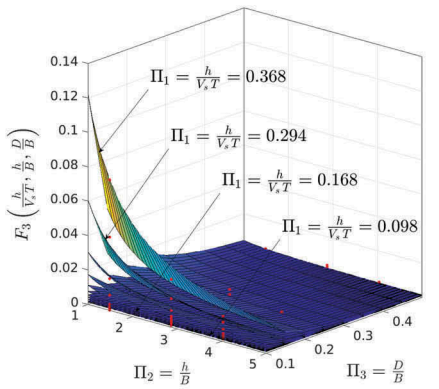

(c) Normalized soil-structure-interaction function $F_3(\hat{\boldsymbol{\pi}}, \hat{\boldsymbol{\alpha}})$ for the horizontal dashpot coefficient c_x.

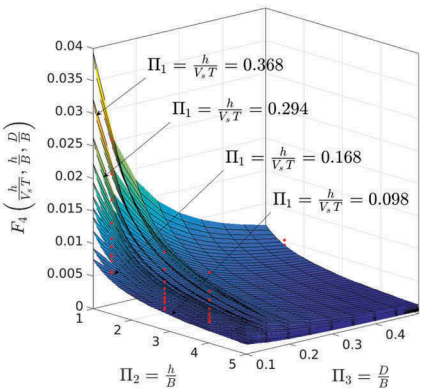

(d) Normalized soil-structure-interaction function $F_4(\hat{\boldsymbol{\pi}}, \hat{\boldsymbol{\alpha}})$ for the vertical dashpot coefficient c_z.

Figure 4. Non-linear curve fitting for the soil-structure-interaction function to the generated data provided with the identified parameters of the 99 analyses.

dimensional parameters; $\hat{\alpha}$ is the vector of non-linear coefficients to be determined from the 99 system identification analyses; and λ_i is the i-th normalizing factor. In particular, non-linear functions $F_i(\hat{\pi}, \hat{\alpha})$ provided in Equation (12) are displayed in Figure 4. In this figure the solid red dots represent the data generated using the sequential optimization method and the surfaces the corresponding performed nonlinear interpolation. A reasonable match is displayed for the four normalized quantities, and the global behavior of the so-generated data is well-represented.

Our validation studies show that the proposed ROM performs very well for transient analyses using real earthquake signals. For instance, Figure 5- 7 show examples of using the derived ROM to compute the building response with a topology shown in the same figure under the Northridge, ChinoHills and Berkeley earthquakes respectively. The first row of Figure 5-7 show the time history of responses in horizontal and vertical directions at the first-modal height, and in horizontal direction at the roof and ground levels. The second row, on the other hand, shows the frequency contents of each signal. As shown, a good-agreement is reached at different building levels. In general, the small discrepancies between the high-fidelity and reduced order models are mostly attributed to

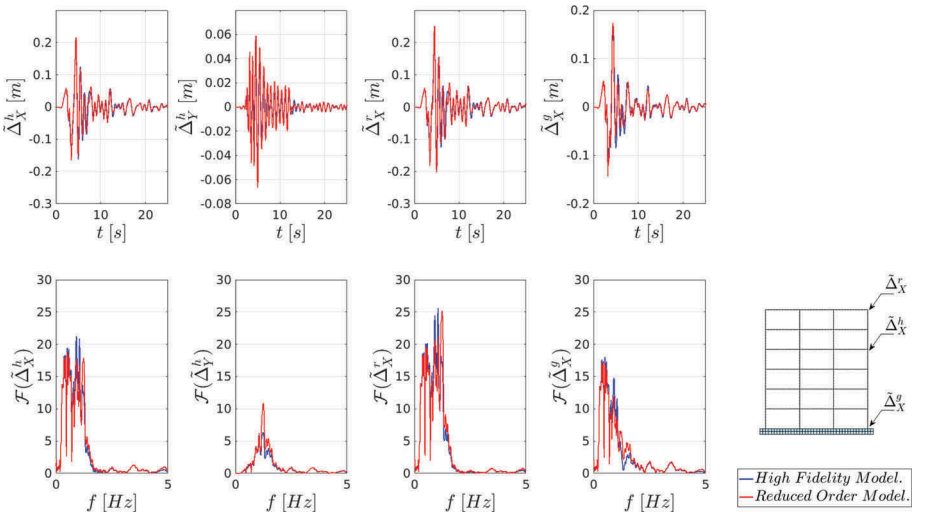

Figure 5. **Frame A:** Subjected to NorthRidge earthquake. The parameters considered in the analysis are for the building a fixed-fundamental period $T = 0.507\,[s]$, and a fixed-first modal height $h = 14.91\,[m]$. The foundation dimensions are a half-width $B = 10\,[m]$, and a foundation depth $D = 1.0\,[m]$. The soil shear velocity is $V_s = 200\,[m/s]$.

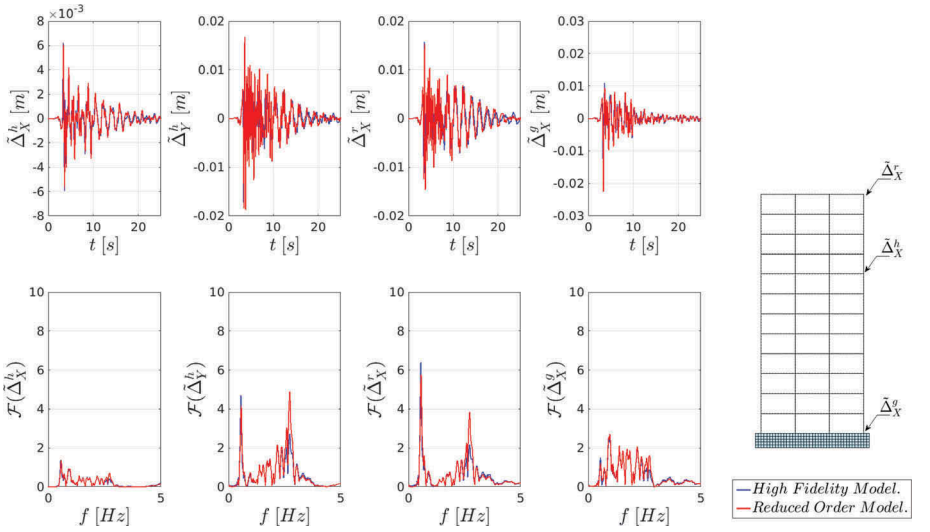

Figure 6. **Frame B:** Subjected to ChinoHills earthquake. The parameters considered in the analysis are for the building a fixed-fundamental period $T = 1.025\,[s]$, and a fixed-first modal height $h = 28.71\,[m]$. The foundation dimensions are a half-length $B = 10\,[m]$, and a foundation depth $D = 2.5\,[m]$. The soil shear velocity is $V_s = 200\,[m/s]$.

the fact that the extrapolation of the soil impedance functions using Equation (12) is first not exact, and second, the number of building frames considered in this analysis to span the whole dimensional parameter space may not be enough; therefore, one can perform a more refined sampling of Π_2 and Π_3 to improve the predictive capability of the ROM.

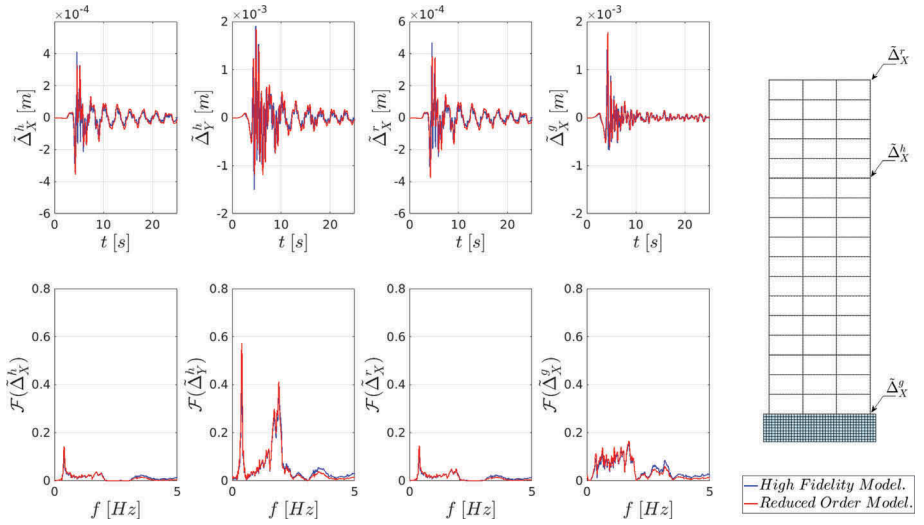

Figure 7. **Frame C:** Subjected to Berkeley earthquake. The parameters considered in the analysis are for the building a fixed-fundamental period $T = 1.531\,[s]$, and a fixed-first modal height $h = 40.36\,[m]$. The foundation dimensions are a half-width $B = 10\,[m]$, and a foundation depth $D = 5.0\,[m]$. The soil shear velocity is $V_s = 200\,[m/s]$.

4 PIPELINES

The physical problem of soil-pipe interaction (SPI) is sophisticated and uncertain, e.g., nonlinear behavior of soil, heterogeneous soil strata, pipe defects, and intrinsically random soil excitation. These complexities and uncertainties rationalize the simplified assumptions. For pipeline analysis, conventionally, beam on nonlinear Winkler foundation (BNWF) models are used, in which pipe and soil are represented by beam and bi-linear spring elements, respectively. The constitutive law for soil springs, known as force-displacement curve (FDC), is well-documented by many researchers and structural design codes, such as API (2002); ALA (2005); PRCI (2009). However, most of the previous work has been using linear or elastic-perfectly plastic idealization of the true nonlinear FDC. On the other hand, the existing FDC is only applicable to monotonic loading, and it fails to capture the hysteresis characteristic of soil in case of cyclic loading, which frequently exists in seismic hazards. Furthermore, their soil springs behave independently with each other in different directions, which does not reflect the coupling nature of soil in response to oblique pipe movement. In this study, we present a two-dimensional (2D) coupled ROM (cf. Figure 8b) to predict the soil-pipe interaction in sand under cyclic and transient loadings (cf. Figure 8). The novelties of this new model are its capability to represent: (1) the true *smooth nonlinear* FDC, (2) *hysteresis loop* of soil response in case of cyclic loading considering the *pinching effect* due to the gap between soil and pipe, and (3) the *coupling* between lateral and vertical soil springs.

To develop the model in a one-dimensional setting, we follow a similar approach as in Varun and Assimaki (2012) and Nguyen and Asimaki (2018) to use a smooth nonlinear FDC to estimate soil reaction force per unit length as follows:

$$F = \alpha K u + (1-\alpha) F_u \zeta \tag{13a}$$

$$\dot{\zeta} = \frac{1}{u_0}\left(1 - \frac{\tanh(\kappa|\zeta|)}{\tanh\kappa}(\beta sign(\dot{u}\zeta) + \gamma)\right)\dot{u} = \frac{1}{u_0} k_{ii}\dot{u} \tag{13b}$$

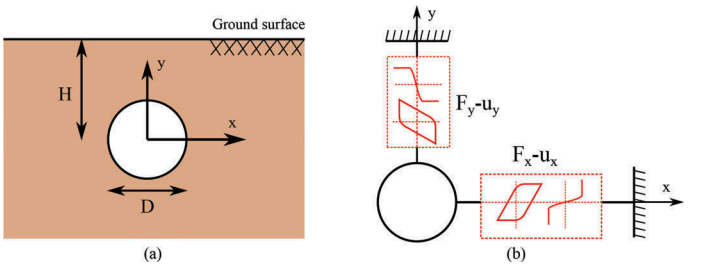

Figure 8. Schematic illustration of the (a) 2D continuum soil-pipe interaction and (b) the proposed reduced order model.

where α is the ratio between post-yield stiffness and initial stiffness of the soil, K is the soil initial stiffness, u is the relative soil-pipe displacement, F_u is the ultimate soil reaction force (yield strength), ζ is the dimensionless hysteresis parameter, $u_0 = F_u/K$, β and γ control the general shape of hysteresis loop ($\beta + \gamma = 1$), and κ controls the smoothness of transition zone of the FDC. We use a sequential optimization method based on unscented Kalman fitering Simon to estimate κ from the FDC of a series of physical experiments available in the literature. We derive κ for lateral and uplift pipe movements in loose, medium, and dense sands, with the embedment ratio in the range $H/D = 1.0 - 12.5$. The results are shown in Figure 9, indicating that κ is larger for softer soil. From physical point of view, softer soil requires larger u to reach F_u. The transition zone is therefore longer and smoother. Furthermore, the similarities in trend and values of κ for lateral and uplift cases suggest that one value of κ is sufficiently accurate to simulate the biaxial SPI problems.

We extend the model from 1D to 2D by incorporating the *coupling* and *pinching* effects. The 2D differential equations for hysteresis parameters are:

$$\dot{\zeta}_x = \frac{1}{u_{0x}(1 + k_{ii}p_\zeta)}(k_{ii}\dot{u}_x - k_{ij}\frac{u_{0x}}{u_{0y}}\dot{u}_y) \tag{14a}$$

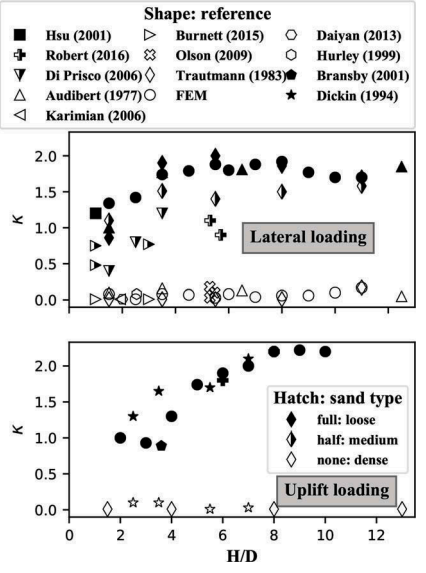

Figure 9. κ for loose sand $I_D = 0 - 35\%$, medium sand $I_D = 35\% - 65\%$, dense sand $I_D = 65\% - 100\%$ for lateral and uplift pipe movement

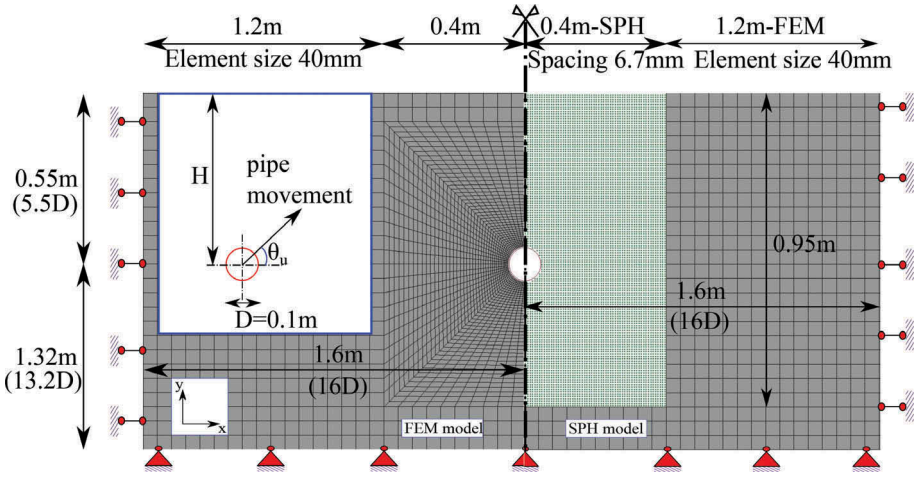

Figure 10. Geometry of the FEM model (left) and SPH model (right) (not to scale)

$$\dot{\zeta}_y = \frac{1}{u_{0x}(1 + k_{ii}p_\zeta)}(k_{ij}\dot{u}_x + k_{ii}\frac{u_{0x}}{u_{0y}}\dot{u}_y) \tag{14b}$$

where u_x, u_y are the relative displacement in x, y axis, $u_{0x} = F_{ux}/K_x$, $u_{0y} = F_{uy}/K_y$, in which F_{ux}, F_{uy}, K_x, K_y are the yield strength and initial stiffness along x and y axis, respectively. The *coupling* effect is quantified by the cross-stiffness term k_{ij}, while the *pinching* phenomenon is controlled by the quantity p_ζ.

The proposed 2D model, hereafter referred to as BMBW model, is verified with the results from *finite element method* (FEM) and *smoothed particle hydrodynamics* (SPH) simulations, of which the fidelity is validated by available experimental data. The geometry mesh and boundary conditions of FEM and SPH model are shown in Figure 10.

The analyses are conducted under different pipe loading patterns: cyclic uniaxial, 0-shape, 8-shape, and Kobe earthquake signal, with small and large displacement amplitude. The bilinear model as in the guidelines of ASCE (1984) is also calculated for the comparison. Due to space limitations, we only present the results of cyclic uniaxial and Kobe earthquake loadings here. The pipe with $D = 100\,[mm]$ is embedded at $H/D = 5.5$ in dry loose Cornell filter sand, having density $\gamma_s = 14.8\,[kN/m^3]$, and plane strain friction angle $\phi'_{crit} = 38.6°$. For comparison purpose, the input parameters F_{ux}, F_{uy}, K_x, K_y of BMBW are directly calibrated from the FEM simulations. As shown in Figure 11, the BMBW is capable of representing the hysteresis loop and pinching effect in case of cyclic loading. For Kobe earthquake signal, the lateral displacement is dominant, and therefore has significant impact on the soil-pipe interaction along

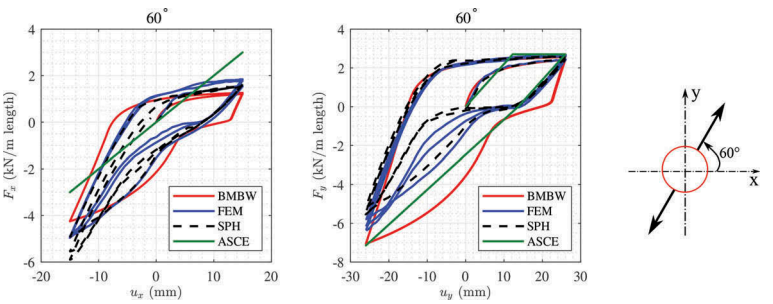

Figure 11. Cyclic uniaxial loading

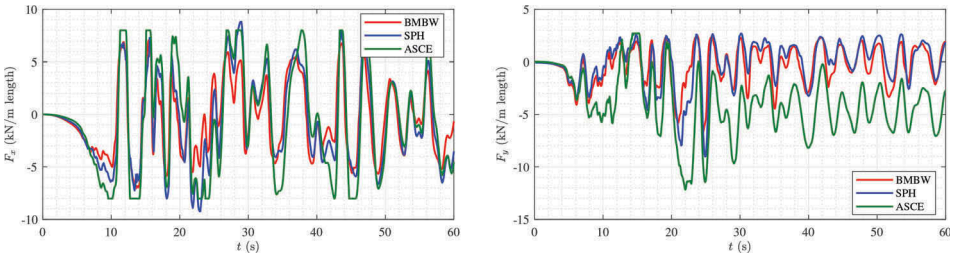

Figure 12. $F_x - t$ and $F_y - t$ under Kobe earthquake loading

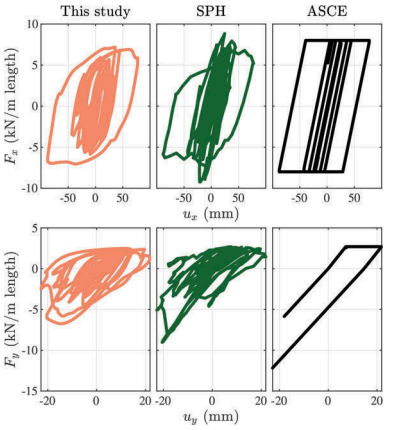

Figure 13. $F_x - u_x$ and $F_y - u_y$ under Kobe earthquake loading

vertical axis. Figure 12 shows that the $F_y - t$ curve from the uncoupled ASCE bilinear approach is shifted compared to that of SPH analysis, while BMBW captures well that coupling effect. As regards the $F_x - u_x$, $F_y - u_y$ curves, as in Figure 13, the shape of FDC from BMBW matches well to that from SPH, with round corners expressing the coupling between lateral and vertical directions.

5 CONCLUSIONS

We have presented three examples of reduced order models (ROMs that we have developed to estimate soil-structure interaction effects. For the case of retaining walls, we adopted dimensional analysis and energy balance, and estimated not only the wall thrust, but more importantly, we revealed that the soil vibrations in the vicinity of the wall comprise a shear and a compressional mode, which emerges due to the presence of the rigid-wall boundary conditions.

To derive the ROM for building foundations, we combined dimensional analysis with EKF, a sequential optimization algorithm through which we identified the functions that best represent the frequency of vibration of the combined soil-foundation-building system. Combining high-fidelity computational models with dimensional analyses, we estimated the coefficients of the uniformly distributed springs and dashpots along the perimeter of the mat foundation that implicitly compensate for kinematic interaction effects due to foundation embedment, if any, and eliminates the need to adopt simplified SSI models and distribute them across the base and sides of the embedded foundation of complex structures. This

particular framework also allows to consider more complicated soil features such as nonlinear material behavior of the soil or loose contact between soil and foundation.

Lastly, we presented a simplified model to predict pipeline response to biaxial loading on a 2D vertical plane. This novel model is able to take into consideration the true smooth nonlinearity, the hysteresis loop, the pinching phenomenon, and the coupling between lateral and vertical displacement. Results of the proposed model show great agreement with numerical simulations FEM and SPH, while reducing considerably the computational effort.

Combining computational models with rigorous methodologies adopted from continuum mechanics, applied mathematics and optimization theory, we have developed physics-based reduced order computational models that achieve efficiency without sacrificing physical intuition and fundamental mechanics.

ACKNOWLEDGEMENTS

The authors would hereby like to thank Prof. Eduardo Kausel at the Massachusetts Institute of Technology, Dr. Craig Davis, Chief Resilience Officer at the Los Angeles Department of Water and Power, and Profs. Michael Ortiz and Andrew Stuart at the California Institute of Technology for their invaluable input to various aspects of this work.

REFERENCES

ALA, A. L. A. (2005). Guidelines for the design of buried steel pipe.

API, A. P. I. (2002). Recommended practice for planning, designing, and constructing fixed offshore platforms-working stress design. *API RP 2A-WSD*.

ASCE, A. S. O. C. E. (1984). Guidelines for the seismic design of oil and gas pipeline systems.

Assimaki, D. (2004). *Topography effects in the 1999 Athens earthquake: engineering issues in seismology*. Ph. D. thesis, Massachusetts Institute of Technology. Dept. of Civil and Environmental Engineering.

Brandenberg, S. J., G. Mylonakis, and J. P. Stewart (2015). Kinematic framework for evaluating seismic earth pressures on retaining walls. *Journal of Geotechnical and Geoenvironmental Engineering 141*(7), 04015031.

Buckingham, E. (1914). *On Physically Similar Systems; Illustrations of the Use of Dimensional Analysis*. Number 4. California Division of Mines and Geology, Office of Strong Motion Studies.: Physical Review.

Gazetas., G. (1991). *Foundation vibrations*. New York, N.Y., Chapman and Hall.: Foundation Engineering Handbook.

Givens, M. J., G. Mylonakis, and J. P. Stewart (2016). Modular analytical solutions for foundation damping in soil-structure interaction applications. *Earthquake Spectra 32*(3), 1749–1768.

Jacobo, B. (1975). Dynamic behaviour of structures with embedded foundations. *Earthquake Engineering & Structural Dynamics 3*(3), 259–274.

Kloukinas, P., M. Langousis, and G. Mylonakis (2012). Simple wave solution for seismic earth pressures on nonyielding walls. *Journal of Geotechnical and Geoenvironmental Engineering 138*(12), 1514–1519.

Lanzano, G., E. Bilotta, G. Russo, F. Silvestri, and S. G. Madabhushi (2012). Centrifuge modeling of seismic loading on tunnels in sand. *Geotechnical Testing Journal 35*(6), 854–869.

Law, K., A. Stuart, and K. Zygalakis (2016). *Data Assimilation: A Mathematical Introduction*. Texts in Applied Mathematics. Springer International Publishing.

Lysmer, J. and R. Kuhlemeyer (1969). *Finite Dynamic Model for Infinite Media*. Reprint (University of California). Department of Civil Engineering, University of California, Institute of Transportation and Traffic Engineering, Soil Mechanics Laboratory.

Nguyen, K. T. and D. Asimaki (2018). A modified uniaxial bouc-wen model for the simulation of transverse lateral pipe-cohesionless soil interaction. In *Geotechnical Earthquake Engineering and Soil Dynamics V*, pp. 25–36.

Pais, A. and E. Kausel (1988). Approximate formulas for dynamic stiffnesses of rigid foundations. *Soil Dynamics and Earthquake Engineering 7*(4), 213–2227.

PRCI, P. R. C. I. (2009). Guidelines for constructing natural gas and liquid hydrocarbon pipelines through areas prone to landslide and subsidence hazards.

Rice, J. R. (1968). A path independent integral and the approximate analysis of strain concentration by notches and cracks. *Journal of applied mechanics 35*(2), 379–386.
Scott, R. (1973). Earthquake-induced pressures on retaining walls. In *Proceedings of the 5th World Conference on Earthquake Engineering*, Volume 2, pp. 1611–1620.
Simon, D. (2006). *Optimal State Estimation: Kalman, H Infinity, and Nonlinear Approaches*. Wiley-Interscience.
Stewart, J., C. Crouse, T. C. Hutchinson, B. Lizundia, F. Naeim, and F. Ostadan. (2012). Soil-structure interaction for building structures.
Stewart, J. P., G. L. Fenves, and R. B. Seed (1999). Seismic soil-structure interaction in buildings. i: Analytical methods. *Journal of Geotechnical and Geoenvironmental Engineering 125*(1), 26–37.
Varun and D. Assimaki (2012). A generalized hysteresis model for biaxial response of pile foundations in sands. *Soil Dynamics and Earthquake Engineering 32*(1), 56–570.
Vazouras, P., S. A. Karamanos, and P. Dakoulas (2010). Finite element analysis of buried steel pipelines under strike-slip fault displacements. *Soil Dynamics and Earthquake Engineering 30*(11), 1361–1376.
Veletsos, A. and J. Meek (1974). Dynamic behaviour of building-foundation systems. *Earthquake Engineering & Structural Dynamics 3*(2), 121–138.
Veletsos, A. S. and A. H. Younan (1994). Dynamic modeling and response of soil-wall systems. *Journal of Geotechnical Engineering 120*(12), 2155–2179.
Weisstein, E. W. Apery‘s constant. From MathWorld—A Wolfram Web Resource. Last visited on 3/1/2019.
Weisstein, E. W. Catalan‘s constant. From MathWorld—A Wolfram Web Resource. Last visited on 3/1/2019.
Wood, J. H. (1973). Earthquake-induced soil pressures on structures.